Persistent Response in an Ultrastrongly Driven Mechanical Membrane Resonator

Fan Yang,[1] Felicitas Hellbach,[1] Felix Rochau,[1] Wolfgang Belzig,[1] Eva M. Weig,[1,2] Gianluca Rastelli,[1,3,*] and Elke Scheer[1,†]

[1]*Fachbereich Physik, Universität Konstanz, 78457 Konstanz, Germany*

[2]*Fakultät für Elektrotechnik und Informationstechnik, Technische Universität München, 80333 München, Germany*

[3]*INO-CNR BEC Center and Dipartimento di Fisica, Università di Trento, 38123 Povo, Italy*

(Received 26 March 2021; revised 1 June 2021; accepted 4 June 2021; published 2 July 2021)

We study experimentally and theoretically the phenomenon of "persistent response" in ultrastrongly driven membrane resonators. The term persistent response denotes the development of a vibrating state with nearly constant amplitude over an extreme wide frequency range. We reveal the underlying mechanism by directly imaging the vibrational state using advanced optical interferometry. We argue that this state is related to the nonlinear interaction between higher-order flexural modes and higher-order overtones of the driven mode. Finally, we propose a stability diagram for the different vibrational states that the membrane can adopt.

DOI: 10.1103/PhysRevLett.127.014304

Mechanical resonators have applications as ultrasensitive sensors of, e.g., molecular transport [1] or as nanomechanical logic gates [2–4]. Nonlinear mechanical properties have come into focus for signal enhancement [5–7] and noise reduction in metrology [8,9] for signal processing. In membrane resonators, different flexural modes can be excited and have been utilized, e.g., for coupling mechanical energy to other degrees of freedom such as light and atoms [10–13]. For micro- and nanomechanical systems in the nonlinear regime, the Duffing model is widely used to describe the vibrational behavior [14,15]. The nonlinearity can be caused by motion-induced tension; i.e., the oscillation of one mode induces an elongation of the resonator that affects the dynamics also of another mode. Hence, for large deflection amplitudes, displacement-induced changes of the mechanical properties may give rise to nonlinear mode coupling [15,16]. Membrane oscillators in the strongly nonlinear regime offer the possibility to explore nonlinear mode coupling mechanisms [14,17–22]. Such coupling leads to exotic line shapes of the response function due to the transfer of energy between mechanical modes that can be faster than the energy relaxation time [20–22].

Here we report a previously undescribed nonlinear behavior achieved in ultrastrongly driven resonators, which occurs when we apply a single sinusoidal drive at a frequency in the range of a flexural mode of a membrane resonator. For simplicity, we concentrate here on the fundamental mode [(1,1) mode]; similar observations have been made for other flexural modes though. Varying the drive frequency, we observe the development of a plateau in the response curves that extends over a considerable frequency range with a nearly constant amplitude; see Fig. 1(a). We denote the almost constant amplitude over an extremely wide frequency range as "persistent response." We argue that this state is maintained by two different interaction mechanisms: nonlinear coupling between different flexural modes and spatial modulation of overtones [22] (i.e., the appearance of frequency multiples of one flexural mode). Here we focus on the first mechanism which becomes progressively dominant at large detuning. In the final part, we make a connection with our previous results recorded in the strong-drive regime [22] to propose a stability diagram for the vibrational state of the membrane and to define the strong and ultra-strong-drive regimes.

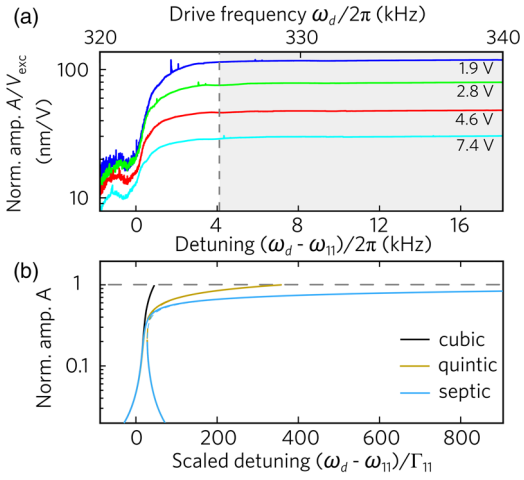

FIG. 1. Persistent response and higher-order nonlinearities. (a) Response function generated by different drive voltages recorded by imaging white light interferometrey showing the mean amplitude response (normalized to the excitation voltage and averaged over the whole membrane area) of the (1,1) mode with eigenfrequency around 321 kHz. (b) Theoretical curves for the amplitude of the (1,1) mode with different higher-order nonlinear forces.

The sample fabrication and measurement principles have been described in detail elsewhere [22–24]. In brief, a chip carrying a high-stress silicon nitride membrane (413.5 μm × 393.5 μm × 478 nm, with residual stress $\sigma = 0.126$ GPa) is glued onto a piezo ring and installed in a vacuum chamber. From the analysis of the linear response, we determine a quality factor around $Q = 20\,000$. Vibrations of the membrane are excited by applying an ac voltage $V_{\mathrm{exc}} \sin(\omega_d t)$ to the piezo resulting in an inertial excitation of the membrane. The vibrational states of a specific (m, n) mode (the integers m and n indicating the number of deflection nodes in the x and y direction) of the membrane are observed by imaging white light interferometry (IWLI), spatially resolving the deflection profile and obtaining the averaged mean amplitude response over the membrane surface area [22,25], and on the other hand, by Michelson interferometry (MI) focusing on one particular position of the membrane with a spot diameter of ~1 μm. Further experimental details are given in Sec. I of the Supplemental Material [26], which includes Refs. [27,28].

We utilize the IWLI signal integrated over the entire membrane area to record the nonlinear vibration behavior under ultrastrong excitation and with a driving frequency ω_d around ω_{11} ($\omega_{11}/2\pi = 321$ kHz, $Q = 20\,000$). Four selected traces revealing the pronounced amplitude saturation recorded for different V_{exc} are plotted over a limited frequency range in Fig. 1(a). The complete frequency-vs-drive map is shown in Fig. S3 in the Supplemental Material [26]. The flattening of the response curve for small detuning above the linear eigenfrequency (here up to 324 kHz) can be described by the spatial modulation of localized overtones as explained in Ref. [22]. Here we concentrate on the frequency range in which the amplitude is almost independent of the drive frequency highlighted by the gray area in Fig. 1(a). At large detuning, we observe features that deviate from the smooth response curve; see below.

By expanding the complex elastic energy potential of the membrane in terms of the normal modes, one generates all possible nonlinear interactions between the different modes. The generic term reads

$$V^{(kh)}_{(nm|\ell p)} = \lambda^{(kh)}_{(nm|\ell p)} q^k_{nm}\, q^h_{\ell p}, \tag{1}$$

with the coupling strength $\lambda^{(kh)}_{(nm|\ell p)}$ where k, h are integers and q_{nm} and $q_{\ell p}$ the amplitudes of the two modes (n, m) and (ℓ, p). Except for some frequency ranges where we observe features that deviate from the smooth curve of the persistent response, we assume the higher-order modes and or the overtones are weakly excited due to nonlinear interaction with the fundamental mode (1,1) such that they oscillate in their linear or Duffing state. However, the dynamics of the higher-order modes affects the response of the driven mode. To illustrate this idea, we discuss a minimal model to qualitatively capture the experimental findings. In this model, we consider the mode (1,1) coupled to the three modes (n, n) with $n = 2$, 3, 4 through the potential $\sum_{n=2}^{4} V^{(n1)}_{(11|nn)} = \sum_{n=2}^{4} \lambda^{(n1)}_{(11|nn)} q^n_{11} q_{nn}$. If the higher-order modes are in the harmonic regime, as shown in Sec. V of the Supplemental Material [26], the dynamic of the fundamental mode driven by a linear force can be described by effective high-order nonlinearities as follows:

$$\begin{aligned}\ddot{q}_{11}(t) = &-\omega^2_{11} q_{11}(t) - 2\Gamma_{11}\dot{q}_{11}(t) + F\cos(\omega_d t) - \gamma_1 q^3_{11}(t) \\ &- \mu_1 q^5_{11}(t) - \nu_1 q^7_{11}(t),\end{aligned} \tag{2}$$

where γ_1 is the Duffing nonlinearity, whereas the quintic and the septic nonlinearities have coefficients $\mu_1 > 0$ and $\nu_1 > 0$. Using the rotating wave approximation (RWA) (see Sec. V of the Supplemental Material [26]), we determine the maximum amplitude and detuning [29]. For a sufficiently strong drive, the vibration amplitude is large and the nonlinear higher-order terms become increasingly important. Figure 1(b) displays that the curve progressively flattens by adding nonlinear self-interaction terms. Furthermore, setting A_{max} as the maximum achievable amplitude at a given drive force, we have that

$$(\omega_{d,\mathrm{max}} - \omega_{11}) = \frac{3\gamma_1}{8\omega_{11}} A^2_{\mathrm{max}} + \frac{5\mu_1}{16\omega_{11}} A^4_{\mathrm{max}} + \frac{35\nu_1}{128\omega_{11}} A^6_{\mathrm{max}}. \tag{3}$$

Figure 2(a) shows an enlargement into the gray-shaded area in Fig. 1(a), where the amplitude is almost independent of the drive V_{exc}. However, nanometer-scale variations are detected in all four curves signaled by small steps and kinks on the plateaus. For $\omega_d < \omega_{22}/2$, we only see the deflection pattern of the (1,1) mode. When $\omega_d \approx \omega_{22}/2$, a (2,2) mode pattern is observed superimposed over the (1,1) mode pattern in the area A. Further increasing ω_d, the (2,3) mode is switched on abruptly and then transitions into the (3,2) mode in the region B. For even larger ω_d, the pattern of the (1,2) mode appears which then switches to the (3,4) pattern at the first shoulder in area C. Before they disappear again, both patterns are observed simultaneously.

The appearance of higher-order modes (m, n) in the deflection profile is a signature of nonlinear mode coupling. Together with the possibility to excite overtones of the individual (m, n) modes [22], we argue that the complex superposition of several modes is generated by an effective nonlinear coupling between different types of modes and overtones. Small continuous deviations from a smooth response curve can qualitatively be described in terms of nonlinear coupling with overtones [22]. Here we discuss the discontinuous steps. They can be explained by an indirect parametric nonlinear interaction mediated by the overtones of the fundamental mode $(m = n)$ or direct

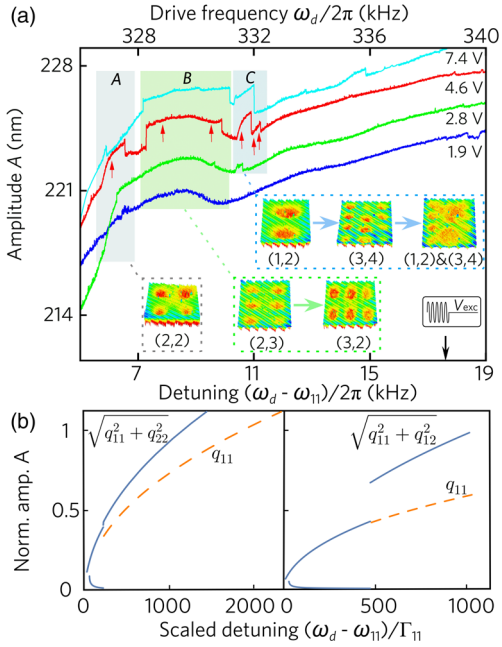

FIG. 2. Persistent response and visualization of deflection patterns. (a) Enlargement of the gray area of Fig. 1(a) without normalizing the y axis. The plateau reveals small steps and kinks superimposed, some of them being marked by colored areas A, B, and C. The red arrows indicate the positions where we captured the deflection patterns for $V_{\mathrm{exc}} = 4.6$ V shown in the insets. The black arrow indicates the frequency at which the ringdown experiments shown in Fig. 4(a) are performed. (b) Numerical solutions of the nonlinear coupling model (solid lines, coupled modes; dashed lines, driven modes). Left: model interaction between the mode (1,1) and the mode (2,2). Right: model interaction between the mode (1,1) and the mode (1,2) (see text for details).

parametric nonlinear interaction between the modes $(m \neq n)$. We discuss two examples to illustrate this idea.

The first example is the indirect interaction of the driven mode (1,1) with the (2,2) mode, with eigenfrequency $\omega_{22} \simeq 2\omega_{11}$. We consider the nonlinear interaction term

$$V^{(22)}_{(11|22)} = \frac{1}{2}\lambda^{(22)}_{(11|22)} q_{11}^2 q_{22}^2 \tag{4}$$

between the two Duffing resonators q_{11} and q_{22} (for simplicity and qualitative analysis, we neglect high-order nonlinearities of the fundamental mode). Because of the presence of an overtone of the fundamental mode, we use the ansatz $q_{11} \simeq (u_1 e^{i\omega_d t} + u_3 e^{i3\omega_d t} + \mathrm{c.c.})/2$ [30]. Then, the mixing term $q_{11}^2 \propto u_1 u_3 e^{i4\omega_d t}$ in Eq. (4) represents the parametric excitation for the high frequency mode (2,2), which becomes resonant and relevant as soon as $4\omega_d \approx 2\omega_{22}$. Using the RWA (see Supplemental Material, Sec. V [26]), we obtain the numerical solutions for the amplitudes of the (1,1) and the (2,2) mode shown in the left panel of Fig. 2(b).

As a second example, we consider the direct interaction between the driven mode (1,1) and the (1,2) mode with eigenfrequency $\omega_{12} \approx (3/2)\omega_{11}$. These modes are described as before as two Duffing resonators for which we have the nonlinear potential

$$V^{(32)}_{(11|12)} = \frac{1}{2}\lambda^{(32)}_{(11|12)} q_{11}^3 q_{12}^2. \tag{5}$$

This parametric interaction becomes resonant and relevant when $3\omega_d \approx 2\omega_{12}$: In the nonlinear interaction Eq. (5), the term $q_{11}^3 \propto u_1^3 e^{i3\omega_d t}$ represents the parametric excitation for the mode (1,2). For this second example, the numerical solution of the amplitudes is shown in the right panel of Fig. 2(b).

To obtain further insight into this nonlinear interaction, ω_d is swept upward from a starting frequency above the linear eigenfrequency (here $\omega_d/2\pi > 326$ kHz) such that the mode (1,1) vibrates in its low-amplitude state. The raw data without any further processing are shown in Fig. 3. For the first example, the curves in Fig. 3(a) show the subharmonic amplitude response of mode (2,2) for different excitation strengths. Figure 3(b) displays a series of power spectra taken during the ringdown of the mode. As

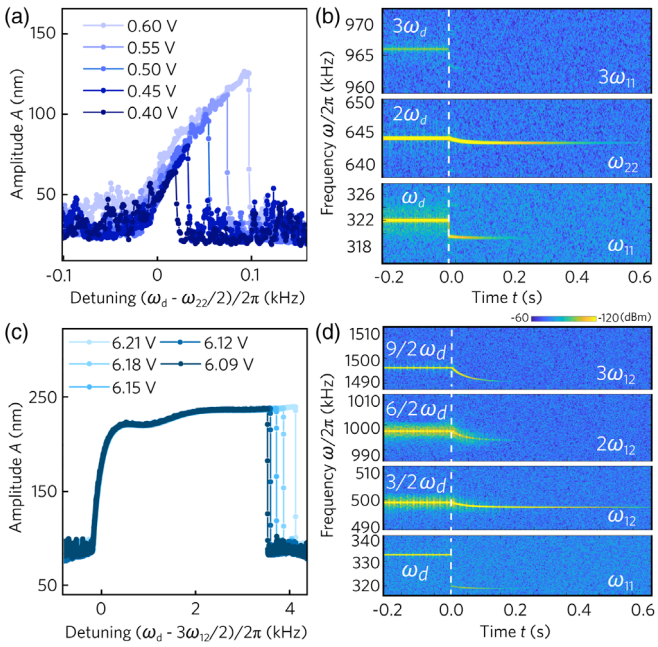

FIG. 3. The subharmonic response functions of the flexural mode (2,2) [(a),(b)] and the mode (1,2) [(c),(d)]. (a) Subharmonic amplitude response of the (2,2) mode. (b) Frequency spectrum of the ringdown for $V_{\mathrm{exc}} = 5.0$ V and $\omega_d/2\pi = 322.0$ kHz (instantly, $\omega_{11}/2\pi = 319$ kHz) showing three integer overtones of ω_d. The drive is turned off at $t = 0$. (c) Subharmonic response of the flexural mode (1,2). (d) Same as (b) but for $V_{\mathrm{exc}} = 7.0$ V and $\omega_d/2\pi = 332.5$ kHz, showing three half-integer overtones of ω_d. The energy decay during ringdown is shown in Sec. IV of the Supplemental Material [26].

soon as the drive has been switched off, the components ω_d and $3\omega_d$ show a jump which is typical for a nonlinear vibration in low-amplitude (harmonic) state. These components can be associated with the fundamental mode with ω_{11} and its odd overtone $3\omega_{11}$ ($\neq \omega_{33}$). On the other side, the components at $2\omega_d$ of the mode (2,2) decay smoothly. Notice that the majority of the power is observed around ω_{22}. All these features are consistent with mode (2,2) being parametrically driven by the mode (1,1) and its odd overtone due to nonlinear coupling according to Eq. (4).

In Fig. 3(c), we show the subharmonic response of the mode (1,2), when the fundamental mode oscillates in the low-amplitude state. Upon increasing ω_d, the amplitude is suddenly pumped up when $V_{\mathrm{exc}} > 6.09$ V. This is characteristic for parametric coupling. Here, the parametric excitation is stronger than in the previous example since the nonlinear interaction with the mode (1,1) in Eq. (5) is direct and not mediated by overtones. The ringdown in Fig. 3(d) is performed for $\omega_d/2\pi = (2/3)\omega_{12}/2\pi = 332.5$ kHz and $V_{\mathrm{exc}} = 7$ V. The corresponding power spectra reveal the half-integer frequencies $(3/2)\omega_d$, $(6/2)\omega_d$, and $(9/2)\omega_d$ which decay to ω_{12}, $2\omega_{12}$, and $3\omega_{12}$ after the drive is switched off. Notice the absence of the overtones of the mode (1,1). Again, these features are consistent with a parametrical drive of the mode (1,2) by the mode (1,1).

As an additional example, we shortly discuss the possible excitation mechanism of the pattern observed in area B of Fig. 2(a): The eigenfrequencies ω_{23} and ω_{32} differ slightly from each other because of the small deviation of the membrane from a square shape. The second overtones of these frequencies $2\omega_{23}/2\pi = 1636$ kHz and $2\omega_{32}/2\pi = 1624$ kHz are close to $5\omega_d$. We therefore argue that these modes are excited subharmonically via nonlinear interaction with the fundamental mode of type $\propto q_{11}^5 q_{23}^2$ or $\propto q_{11}^5 q_{32}^2$.

We will now turn to the analysis of the persistent response of the (1,1) mode. We repeat the experiment shown in Fig. 1(a) to explore the frequency response and the ringdown behavior of the membrane subject to an ultrastrong excitation $V_{\mathrm{exc}} = 5.0$ V at $\omega_d/2\pi = 338.6$ kHz marked as black arrow in Fig. 2(a), well above ω_{11} using MI. With the excitation switched off ($t = 0$), the time-resolved power spectrum recorded in the frequency range 250 kHz to 2.5 MHz displayed in Fig. 4(a) shows the contribution of ω_d and its overtones up to sixth order. Owing to the detuned drive ($n\omega_d \neq \omega_{nn}$), the frequency of the individual contributions shifts toward a nearby eigenfrequency of the membrane [31,32]. By comparison with the eigenfrequencies, the most prominent modes are identified as (i) flexural modes with $m = n$ and their overtones [e.g., the second overtones of the modes (1,1) and (2,2)]; (ii) flexural modes with $m \neq n$, here the second overtone of the (2,3) and the (3,2) modes and the fourth overtone of the (1,2) mode; (iii) mixed-frequency response

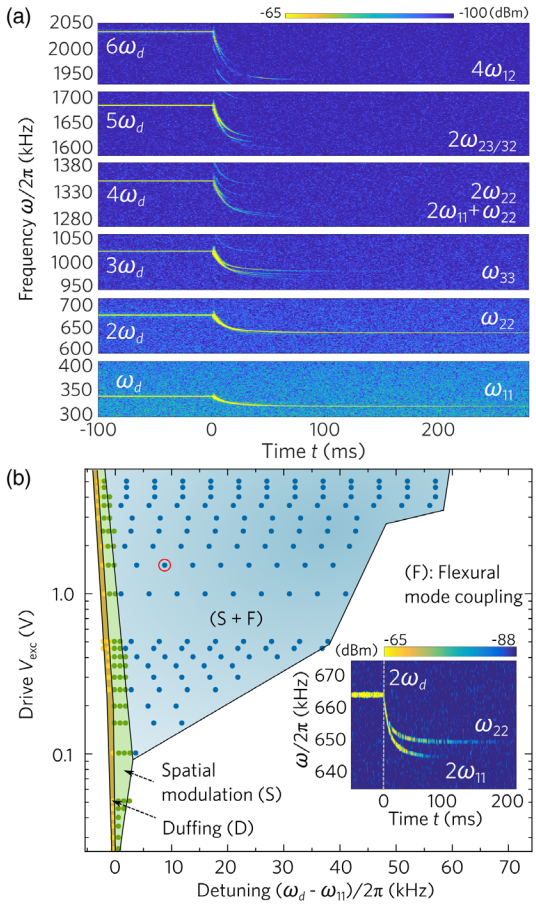

FIG. 4. Ringdown measurement in the flexural mode coupling regime. (a) Frequency spectrum of the ringdown for $V_{\mathrm{exc}} = 5$ V and $\omega_d = 338.6$ kHz showing six overtones of ω_d. The drive is turned off at $t = 0$. For details of the mode assignment and energy decay, see Sec. IV in the Supplemental Material [26]. (b) Stability diagram of the vibrational state of the membrane resonator as a function of the detuning from ω_{11} and drive V_{exc}. The solid lines are determined by combining experimental data from MI (colored dots) and IWLI data shown in Fig. S3 in the Supplemental Material [26]. The inset shows an example of a coexistence of flexural mode coupling and spatial overtones [22]: ringdown recorded for $V_{\mathrm{exc}} = 1.77$ V at $\omega_d/2\pi = 331$ kHz (marked by a red circle in the main panel) showing a frequency splitting into ω_{22} and $2\omega_{11}$.

such as $2\omega_{11} + \omega_{22}$ in the decay of $4\omega_d$ (the detailed identification of the mixed-frequency modes is shown in the Supplemental Material, Sec. IV [26]).

Finally, combining the findings in the various regimes enables us to establish a tentative stability diagram of the complex vibrational behavior of the persistent response of the membrane resonator, as shown in Fig. 4(b). When increasing the excitation strength beyond the linear response regime (weak drive), a gradual transition to the Duffing behavior occurs (medium drive, yellow-shaded area, denoted as D). This behavior persists up to very high drive, but in a very small detuning range. For even larger

V_{exc} and increasing detuning, the spatial modulation regime with overtones sets in and can be observed up to very high drive, but narrow detuning range. We denote this green-shaded area labeled S as the strong-drive condition. Above a certain drive strength and detuning, a new state appears in which flexural mode coupling and spatially modulated overtones are observed simultaneously (blue-shaded area labeled $S + F$, as exemplified in the inset). Here, a ring-down experiment is shown for the conditions marked with a red circle in the main panel. After turning off the drive, the components at $2\omega_d$ split into two branches that decay into the $2\omega_{11}$ and ω_{22} frequencies, namely, to one higher flexural mode and to one spatial overtone of the fundamental mode. The appearance of the flexural modes defines the ultra-strong-drive regime.

Summarizing, by combination of two complementary experimental approaches and with nonlinear coupling models, we described the observation of persistent response of the membrane resonator and revealed unconventional nonlinear interaction between the driven fundamental mode, its overtones, and higher-order flexural modes, which occurs under ultrastrong drive. This persistent response state has, in the example shown here, an extension of more than 50% of the eigenfrequency of the driven mode, but even longer plateaus are shown in the Supplemental Material, Sec. III [26]. Hence, ultrastrongly driven membranes lend themselves to be utilized as adaptive resonators without actively tuning their eigenfrequency, e.g., for energy transfer to resonating systems with different degrees of freedom. We argue that the observed phenomena might become even more pronounced when increasing the Q factor by using thinner membranes. We expect that our findings will help clarify other unusual phenomena appearing in strongly nonlinear systems, also beyond the mechanical case.

The authors thank J. S. Ochs and A. Brieussel for their contributions in the early stage of the work. We are indebted to T. Dekorsy, V. Gusev, M. Hettich, P. Leiderer, M. Fu, and Y. Jiang for fruitful discussion and comments about the work. The authors gratefully acknowledge financial support from the China Scholarship Council, the European Union's Horizon 2020 program for Research and Innovation under Grant Agreement No. 732894 (FET Proactive HOT), the Deutsche Forschungsgemeinschaft (German Research Foundation) through Project-ID No. 32152442—SFB 767 and Project-ID No. 425217212—SFB 1432, and from the German Excellence Strategy via the Zukunftskolleg of the University of Konstanz.

*gianluca.rastelli@ino.cnr.it
†elke.scheer@uni-konstanz.de

[1] B. Arash, J.-W. Jiang, and T. Rabczuk, A review on nanomechanical resonators and their applications in sensors and molecular transportation, Appl. Phys. Rev. **2**, 021301 (2015).
[2] I. Mahboob and H. Yamaguchi, Bit storage and bit flip operations in an electromechanical oscillator, Nat. Nanotechnol. **3**, 275 (2008).
[3] D. N. Guerra, A. R. Bulsara, W. L. Ditto, S. Sinha, K. Murali, and P. Mohanty, A noise-assisted reprogrammable nanomechanical logic gate, Nano Lett. **10**, 1168 (2010).
[4] Y. Tadokoro and H. Tanaka, Highly Sensitive Implementation of Logic Gates with a Nonlinear Nanomechanical Resonator, Phys. Rev. Applied **15**, 024058 (2021).
[5] D. Rugar and P. Grütter, Mechanical Parametric Amplification and Thermomechanical Noise Squeezing, Phys. Rev. Lett. **67**, 699 (1991).
[6] R. B. Karabalin, R. Lifshitz, M. C. Cross, M. H. Matheny, S. C. Masmanidis, and M. L. Roukes, Signal Amplification by Sensitive Control of Bifurcation Topology, Phys. Rev. Lett. **106**, 094102 (2011).
[7] L. Papariello, O. Zilberberg, A. Eichler, and R. Chitra, Ultrasensitive hysteretic force sensing with parametric nonlinear oscillators, Phys. Rev. E **94**, 022201 (2016).
[8] A. Chowdhury, M. G. Clerc, S. Barbay, I. Robert-Philip, and R. Braive, Weak signal enhancement by nonlinear resonance control in a forced nano-electromechanical resonator, Nat. Commun. **11**, 2400 (2020).
[9] J. S. Huber, G. Rastelli, M. J. Seitner, J. Kölbl, W. Belzig, M. I. Dykman, and E. M. Weig, Spectral Evidence of Squeezing of a Weakly Damped Driven Nanomechanical Mode, Phys. Rev. X **10**, 021066 (2020).
[10] S. Camerer, M. Korppi, A. Jöckel, D. Hunger, T. W. Hänsch, and P. Treutlein, Realization of an Optomechanical Interface between Ultracold Atoms and a Membrane, Phys. Rev. Lett. **107**, 223001 (2011).
[11] R. W. Andrews, R. W. Peterson, T. P. Purdy, K. Cicak, R. W. Simmonds, C. A. Regal, and K. W. Lehnert, Bidirectional and efficient conversion between microwave and optical light, Nat. Phys. **10**, 321 (2014).
[12] A. Jöckel, A. Faber, T. Kampschulte, M. Korppi, M. T. Rakher, and P. Treutlein, Sympathetic cooling of a membrane oscillator in a hybrid mechanical-atomic system, Nat. Nanotechnol. **10**, 55 (2015).
[13] T. M. Karg, B. Gouraud, C. T. Ngai, G.-L. Schmid, K. Hammerer, and P. Treutlein, Light-mediated strong coupling between a mechanical oscillator and atomic spins 1 meter apart, Science **369**, 174 (2020).
[14] A. H. Nayfeh and D. T. Mook, *Nonlinear Oscillations* (John Wiley & Sons, New York, 2008).
[15] R. Lifshitz and M. C. Cross, in *Reviews of Nonlinear Dynamics and Complexity*, edited by H. G. Schuster (John Wiley & Sons, New York, 2008).
[16] H. J. R. Westra, M. Poot, H. S. J. vander Zant, and W. J. Venstra, Nonlinear Modal Interactions in Clamped-Clamped Mechanical Resonators, Phys. Rev. Lett. **105**, 117205 (2010).
[17] A. I. Manevich and L. I. Manevitch, *The Mechanics of Nonlinear Systems with Internal Resonances* (World Scientific, Singapore, 2005).
[18] F. Mangussi and D. H. Zanette, Internal resonance in a vibrating beam: A zoo of nonlinear resonance peaks, PLoS One **11**, e0162365 (2016).

[19] O. Shoshani, S. Shaw, and M. Dykman, Anomalous decay of nanomechanical modes going through nonlinear resonance, Sci. Rep. **7**, 18091 (2017).

[20] J. Güttinger, A. Noury, P. Weber, A. M. Eriksson, C. Lagoin, J. Moser, C. Eichler, A. Wallraff, A. Isacsson, and A. Bachtold, Energy-dependent path of dissipation in nanomechanical resonators, Nat. Nanotechnol. **12**, 631 (2017).

[21] C. Chen, D. H. Zanette, D. A. Czaplewski, S. Shaw, and D. López, Direct observation of coherent energy transfer in nonlinear micromechanical oscillators, Nat. Commun. **8**, 15523 (2017).

[22] F. Yang, F. Rochau, J. S. Huber, A. Brieussel, G. Rastelli, E. M. Weig, and E. Scheer, Spatial Modulation of Nonlinear Flexural Vibrations of Membrane Resonators, Phys. Rev. Lett. **122**, 154301 (2019).

[23] R. Waitz, S. Nößner, M. Hertkorn, O. Schecker, and E. Scheer, Mode shape and dispersion relation of bending waves in thin silicon membranes, Phys. Rev. B **85**, 035324 (2012).

[24] F. Yang, R. Waitz, and E. Scheer, Quantitative determination of the mechanical properties of nanomembrane resonators by vibrometry in continuous light, arXiv:1704.05328.

[25] S. Petitgrand, R. Yahiaoui, K. Danaie, A. Bosseboeuf, and J. Gilles, 3d measurement of micromechanical devices vibration mode shapes with a stroboscopic interferometric microscope, Opt. Lasers Eng. **36**, 77 (2001).

[26] See Supplemental Material at http://link.aps.org/supplemental/10.1103/PhysRevLett.127.014304 for details of the sample preparation and the measurement methods, characterization measurements of the membrane under study, examples of subharmonic parametric resonance phenomena observed for different flexural modes, the identifications of mode frequency mixing, the energy decay results of the ringdown process, and the detailed description of the theoretical models.

[27] R. Waitz, C. Lutz, S. Nößner, M. Hertkorn, and E. Scheer, Spatially Resolved Measurement of the Stress Tensor in Thin Membranes Using Bending Waves, Phys. Rev. Applied **3**, 044002 (2015).

[28] X. Zhang, R. Waitz, F. Yang, C. Lutz, P. Angelova, A. Gölzhäuser, and E. Scheer, Vibrational modes of ultrathin carbon nanomembrane mechanical resonators, Appl. Phys. Lett. **106**, 063107 (2015).

[29] Note that the inclusion of higher-order terms causes still three possible solutions in the parameter regime of the experiment, two stable and an unstable one, as in the Duffing case, not shown in in Fig. 1(b).

[30] The first overtone at $2\omega_d$ is also present and couples to another higher-order mode; see Sec. IV of the Supplemental Material SM for further examples.

[31] T. Antoni, K. Makles, R. Braive, T. Briant, P.-F. Cohadon, I. Sagnes, I. Robert-Philip, and A. Heidmann, Nonlinear mechanics with suspended nanomembranes, Europhys. Lett. **100**, 68005 (2012).

[32] P. M. Polunin, Y. Yang, M. I. Dykman, T. W. Kenny, and S. W. Shaw, Characterization of MEMS resonator nonlinearities using the ringdown response, J. Microelectromech. Syst. **25**, 297 (2016).